AL53 - Modeling of the Distribution of Alumina Aggregates in an Electrolysis Cell based on a Multi-Slice Method

Thomas Roger[1], Lukas Dion[1], Laszlo Kiss[1], Patrice Chartrand[2], Sébastien Guérard[3] and Jean-François Bilodeau[3]

1. GRIPS, Université du Québec à Chicoutimi, Chicoutimi, Canada
2. Polytechnique Montréal, Montréal, Canada
3. Arvida Research and Development Center, Rio Tinto Aluminium, Jonquière, Canada

Corresponding author: troger@uqac.ca

Abstract

Uneven alumina distribution is one of the factors that may disrupts the stability of electrolysis cells. Consequently, an improved understanding of the mechanisms leading from the alumina injection to its complete dissolution will reduce environmental impact (lower greenhouse gas (GHG) emissions) and improve the lifespan of the cells (improved stability with fewer thermal excursions). When alumina is injected, a layer of bath solidifies around the powder due to the decrease in temperature, forming an agglomerate, or a raft. This raft will undergo fragmentation that forms additional aggregates and each of these will contribute to alumina dissolution in different regions of the electrolytic cells until completely dissolved. It is considered that each alumina-bath agglomerate can only be in one of three specific states: 1) it can float on the surface of the bath, 2) sink in the bath and relocate at the bath-metal interface, or 3) settle on the cathode surface and contribute to the formation of alumina sludge.

This article presents a model for tracking the movement of aggregates in the electrolysis cell. The objective is to highlight the most likely alumina distribution patterns and to identify areas with low alumina feed and areas more prone to sludge formation. The model is based on three independents layers: the free surface of the bath, the bath-metal interface (BMI), and the cathode surface. Each layer has their own respective flow and agglomerates population along with specific behavior and criteria which allow the passage of one state to another. By comparing different simulations, the article highlights the main factors that contribute to atypical alumina dissolution pattern, uneven alumina distribution and increased sludge formation. Consequently, this study pinpoints areas of improvements for primary aluminum production to mitigate the effect of these drawbacks.

Keywords: Alumina distribution; Raft formation; Mathematical model; Sludge formation; Alumina dissolution.

1. Introduction

Aluminum is a highly valued material in various fields due to its mechanical, thermal, and electrical properties. The production of aluminum is achieved through electrolysis in a cell filled with an electrolyte, generally referred to as bath. The metal produced is then accumulating at the bottom of the cell as molten aluminum. Under such circumstances, three interfaces can be distinguished: the surface of the bath in contact with free-air, bath-metal interface (BMI), and the surface of the carbon cathode in contact with the metal. Alumina is injected into the cells in the form of a granular material. Since the injected alumina temperature is much lower than the solidification temperature of the bath, bath infiltrates through the particles and solidifies around and within the alumina powder to form an agglomerate called a raft. This entity generally floats on the free surface of the bath until it disintegrates or dissolves completely. In the case of disintegration, the aggregates sink to the bath-metal interface. Depending on their geometry, the aggregates will either float on the BMI or perforate it and migrate to the surface of the cathode to

form sludge. The presence of this sludge on the cathode surface affects the flow of current and the stability of the cell. The distribution of dissolved alumina is also influenced by the movement of rafts at the free surface of the bath and the bath-metal interface due to their dissolution process. This article presents the development of a model created to track the position and behavior of rafts and agglomerates in the electrolysis cell.

The present model consists of simulating three parallel plane surfaces. One simulates the bath flow at the free surface of the bath, the second simulates the different mechanisms at the bath-metal interface, and the third plane simulates the liquid aluminum a few centimeters above the cathode surface. The flows are based on results from computational fluid dynamics (CFD) simulations and the resulting flow profile is implemented directly in the mathematical model.

Dissolution and disintegration of the rafts and agglomerates are based on a heuristic model developed through a collaborative research [1]. This work was developed using the main elements from the fundamental thermodynamics of the dissolution process coupled with observations and measurements conducted under industrial and laboratory conditions. Hence, with known cell conditions, it is possible to predict the total length of the dissolution process for each individual raft or agglomerate.

By reproducing the physics associated to these alumina-bath agglomerates with a known lifetime which are immerged into different liquids flows with known properties and velocity; the proposed model allows for the precise tracking of the position of each raft and agglomerate until their complete dissolution. The choice of importing results from external numerical model was selected to reduce computation time and to enhance the potential of the model to simulate a wide variety of cell conditions rapidly.

2. Methodology

2.1 Presentation of the Multi-Slice Model

Homogeneity of alumina concentration in electrolysis cells is crucial to maintain the proper balance that assures stability in current distribution (limiting the formation of perfluorocarbons (PFC)), while mitigating the risk formation of sludge on the cathode surface. As described in the introduction, the multi-slice model's main goal is to represent the different interfaces in aluminum electrolysis cells in order to track the movement of alumina rafts and aggregates. By understanding the behavior of the undissolved alumina, this tool can target areas of the bath where undissolved alumina is more likely to be present; leading to a significant contribution to the local alumina concentration of these regions while also determining areas prone to sludge accumulation on the cathode surface.

Several models [2-8] simulate the movement of the rafts in the cell using the CFD method to determine the flow related to magnetohydrodynamic (MHD) forces. Bojarevics et al. [4] presented a follow-up of aggregates of different sizes at the bath-metal interface with the transport being exclusively controlled by the MHD flow. Bojarevics et al. [4] show that the deformation of the interface has a significant impact on the movement of the rafts. Liu et al. [3] considered that the injection of alumina would create small agglomerates with a diameter of approximately five centimeters. These two papers don't consider the displacement of the raft at the free surface of the bath, which can be significant as reported by some authors [9-11]. Rakotondramanana et al. and Richer et al. presented an novel approach by studying the tranport of agglomerates specifically at the BMI interface. These papers inspired the work presented in this paper.

2.1.1 Free Surface of the Bath: General Flow

The flow at the free surface of the bath is influenced by MHD effects as well as the flow of bubbles near the anodes. In order to maximize the running speed of the model, the flow is not coupled within the multi-slice model and is rather imported from external simulation. In this case, the flow at the free surface of the bath was simulated using the COMSOL Multiphysics® software [12]. The steady flow considered throughout the simulation is represented in the Figure 1.

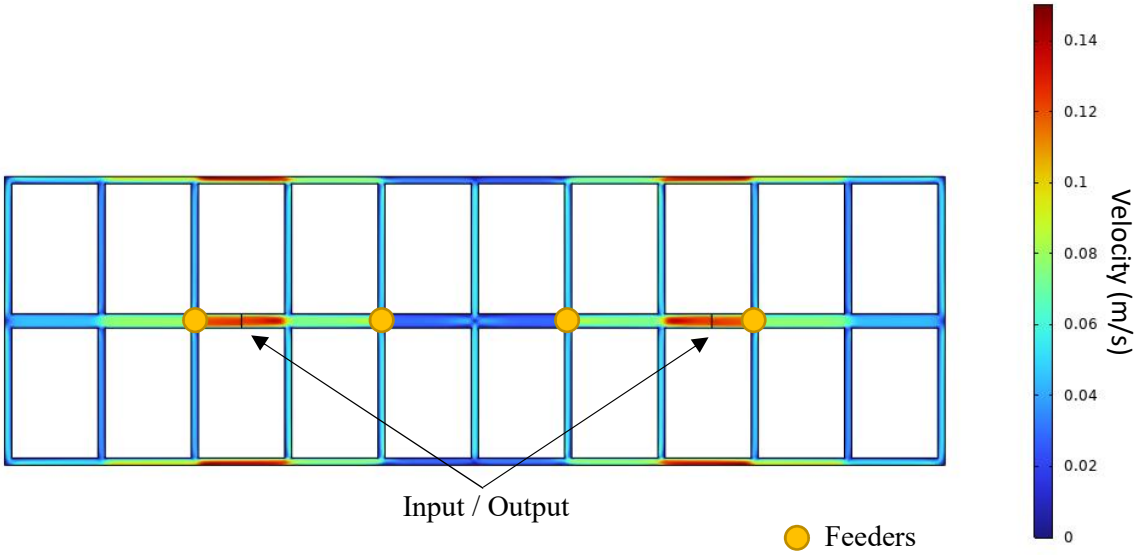

Figure 1. Flow pattern at the bath free surface.

In order to create the flow, an inlet and an outlet are placed at the quarter and three-quarter positions of the cell in the horizontal direction, as shown in the Figure 1. The flow is imposed at the inlet with an average velocity of 10 cm/s [13] and zero relative pressure at the outlets (see Figure 2).

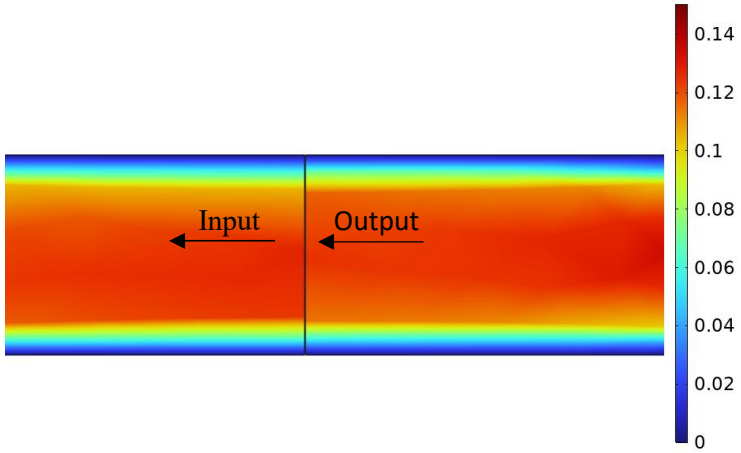

Figure 2. Method used to simulate the flow at the bath free surface.

2.1.2 Bath-Metal Interface: Effect of the Waves and Deformation

The mathematical model considered in this slice is based on a model developed by Richer et al. [5] that simulates the transport of rafts at the BMI. The model presented a methodology for simulating the interface with a superposition of three different phenomena: the permanent deformation related to magnetohydrodynamic (MHD) forces, the deformation of the interface in the form of waves and the general flow also related to MHD forces. The original work by Richer

et al. only considered the representation of the BMI by simulating transiently the distortion of the interface with a permanent deformation coupled to different wave profiles. The developments proposed in this article consider the exchanges between different vertical slices, leading to different time and location for the injection points of the aggregates at the BMI. The multi-slice model also considers a superposition of the different mechanisms occurring at the BMI layer, but these concepts are presented separately for an easier comprehension.

Refinements were performed to the wave deformation of the interface to more accurately account for the typical waves pattern observed in industrial cells with a wave period of 40 seconds. The sum of the final deformation is illustrated in Figure 3 and follows at two different time instants.

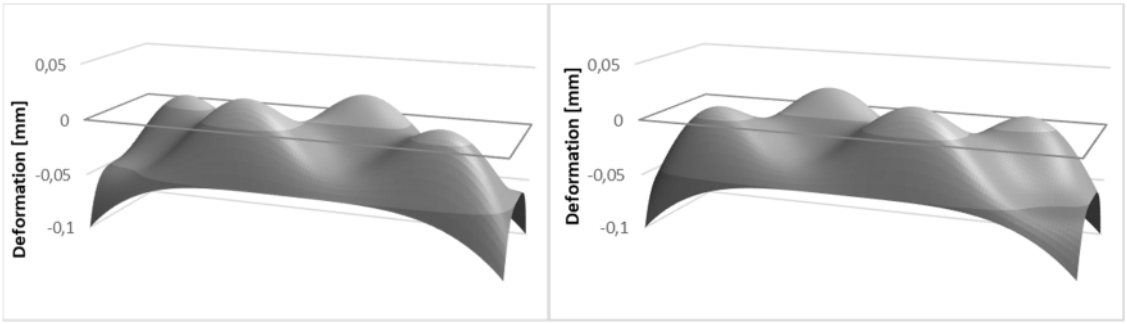

Figure 3. Deformation of the BMI at 10 s and 30 s.

The equation used to generate permanent deformation (D_{perm}) is as follows:

$$D_{perm} = A\left(x - \frac{L_x}{2}\right)^4 + B\left(y - \frac{L_y}{2}\right)^4 \quad (1)$$

where:

$$A = -\frac{\frac{P_{max}}{2}}{\left(\frac{L_x}{2}\right)^4} \quad et \quad B = -\frac{\frac{P_{max}}{2}}{\left(\frac{L_y}{2}\right)^4} \quad (2)$$

where:

x Horizontal coordinate, m
y Vertical coordinate, m
L_x Length of the cell, m
L_y Width of the cell, m
P_{max} Maximum deformation of the interface in the corners of the cell, m.

The maximum deformation is fixed at 10 cm corresponding to the half of the metal depth [14]. The deformation associated with interface fluctuations forming waves is generated using the following equation:

$$D_{cell} = \frac{A}{2}\sin\left(\frac{4\pi\left(x - \frac{L_x}{2}\right)}{L_x}\right)\sin\left(\frac{2\pi\left(y - \frac{L_y}{2}\right)}{L_y}\right)\sin(\omega t) \quad (3)$$

where:

A Amplitude of the deformation, m
ω Resonance frequency, rad/s

t Time, s.

The amplitude is set to 5 cm, and the frequency is fixed for a period of 40 seconds.

2.1.3 Flow Pattern at the Bath-Metal Interface

The flow at the BMI is governed by the magnetohydrodynamic (MHD) force as the resulting flow acts on the raft via the drag force. Similar to simulating the free surface of the bath, an imposed velocity field is used throughout the simulation. In this case, the results were interpolated from a flowchart map provided by our industrial partner which was obtained from MHD simulations. Figure 4 shows the velocity field used, which represents two symmetric vortices with respect to each other in the horizontal direction. The authors acknowledge that the flow is not perfectly symmetric in real cells but this simplification was chosen as a reference scenario facilitate the implementation of the velocity field. Studies on the effect of the flow pattern resulting from different operating conditions will be the subject of future research.

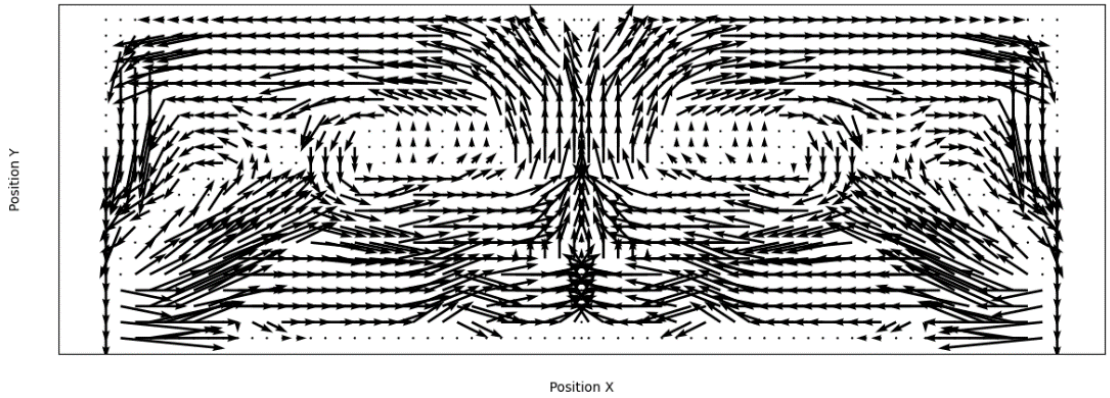

Figure 4. Velocity field of the MHD flow.

2.1.4 Cathode-Aluminium Slice: General Flow

The flow at the cathode surface is similar at the MHD flow at BMI. The difference with the BMI is the flat surface. There is no wave-deformation of the cathode surface. It also disregards the effect caused by an uneven cathode surface; thus, it is applicable on the early life of the cell and additional considerations should be accounted for to correct the flow for cells with considerable uneven cathode erosion.

2.1.5 Interslice Movement

The rafts are created at the free surface of the bath below the injector with a 15-second delay between each injection. The heuristic model is then presented and allows determining the fragmentation of the raft to form agglomerates that will position themselves at the bath-metal interface. Following the movement of the agglomerates to the BMI, if they end up in a corner of the cell, they migrate to the surface of the cathode.

2.2 Balance of Forces

The movement of the raft is resolved with the Newton's second law and drive by the contact force between raft, the drag force, the buoyancy force and the gravity like show on the Figure 5.

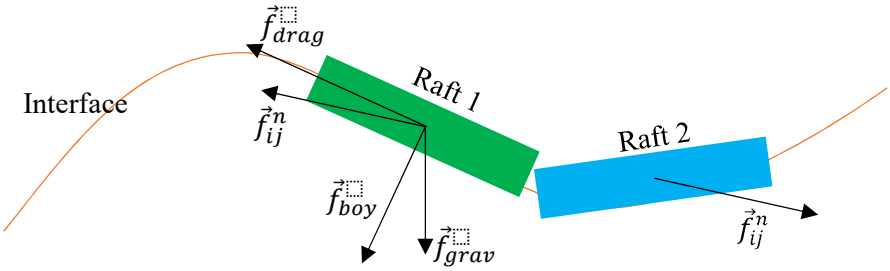

Figure 5. Balance of force applied in the raft.

where:

$\vec{f}_{ij}^{n}$ Contact force, N
$\vec{f}_{drag}$ Drag force, N
$\vec{f}_{boy}$ Buoyancy force, N
$\vec{f}_{grav}$ Gravity force, N

2.2.1 The Contact Force

During an impact between two rafts, a contact force ($\vec{f}_{ij}^{n}$) based on a viscoelastic model is applied to avoid any overlap. This equation is used by the discrete element method. This force is applied to all rafts and chunks in all layers of the cell. The equation is proposed by Belytschko et al. [15]:

$$\vec{f}_{ij}^{n} = \vec{f}_{el}^{n} + \vec{f}_{diss}^{n} = (k_c\delta_n + \eta_c\dot{\delta}_n)\vec{n}_{ij} \quad (4)$$

where:

$\vec{f}_{el}^{n}$ Elastic component, N
$\vec{f}_{diss}^{n}$ Damping component, N
k_c Contact coefficient
δ_n Interpenetration, m
η_c Damping coefficient
$\dot{\delta}_n$ Velocity of interpenetration, m/s
$\vec{n}_{ij}$ Normal vector of the contact.

2.2.2 The Drag Force

The drag force ($\vec{f}_{drag}$) represents the friction between the raft and the various liquids. The equation used is different at the surface of the bath, the surface of the cathode, and the bath-metal interface. Since the air above the bath is not considered, the BMI is the only interface that considers two liquids. For the surface of the bath and the surface of the cathode, the equation used is as follows:

$$\vec{f}_{drag} = \frac{1}{2}\rho C_d \pi r^2 h\left(\vec{v}_{liq} - \vec{v}_{raft}\right)^2 \quad (5)$$

where:

ρ Density of the fluid acting on the raft (that of the bath at the free surface and that of the liquid aluminum at the surface of the cathode), kg/m^3
C_d Drag coefficient

r Radius of the raft, m
h Height of the raft, m
$\vec{v}_{liq}$ Velocity of the fluid, m/s
$\vec{v}_{raft}$ Velocity of the raft, m/s.

The equation of the drag force at the bath-metal interface becomes:

$$\vec{f}_{drag} = \frac{1}{2} C_d \pi r^2 (\rho_{bath} h_1 + \rho_{alu} h_2)(\vec{v}_{liq} - \vec{v}_{raft})^2 \quad (6)$$

where:
ρ_{bath} Density of the bath, kg/m^3
h_1 Height of the raft in the bath, m
ρ_{alu} Density of the aluminum, kg/m^3
h_2 Height of the raft in the aluminum, m.

2.2.3 Buoyancy Force

The buoyancy force is applied only at the BMI. It determines the position of the raft with respect to the interface and transfers the energy from the waves and interface deformation to the acceleration of the raft.

$$\vec{f}_{boy} = \pi r^2 (\rho_{bath} h_1 + \rho_{alu} h_2) g \vec{n}_{inter} \quad (7)$$

where:
g Gravity acceleration, m/s^2
$\vec{n}_{inter}$ Normal vector of the interface.

2.2.4 Gravity Force

The last force applied on the raft is the gravity force:

$$\vec{f}_{grav} = \pi r^2 \rho_{raft} h_{raft} \vec{g} \quad (8)$$

where:
$\vec{g}$ Gravity acceleration vector, m/s^2
ρ_{raft} Density of the raft, kg/m^3
h_{raft} Height of the raft, m.

2.3 Heuristic Alumina Dissolution Model

The heuristic model was developed through a collaborative research between different organizations [1]. This model is based on the description of the life cycle of an alumina raft, relying on the thermodynamical considerations combined with observations and measurements taken on rafts after their injection into the electrolysis cells [9-11, 16, 17]. This approach allowed for the description of raft fragmentation and dissolution while considering the mass of solidified bath and the properties of the bath. The following Figure 6 shows the predicted evolution of the mass of a raft over its lifetime. An initial increase is due to the agglomeration of alumina and solidified bath, and the following decrease is a superposition of the phase change of the bath, the dissolution of the alumina and the disintegration of the raft. The amount fed, the alumina temperature, the bath chemistry and bath temperature are input variables that will affect the

predicted outcome. Figure 6 illustrates an example of the predicted mass of the alumina raft following an injection of 1 kg of alumina, under a specific set of conditions.

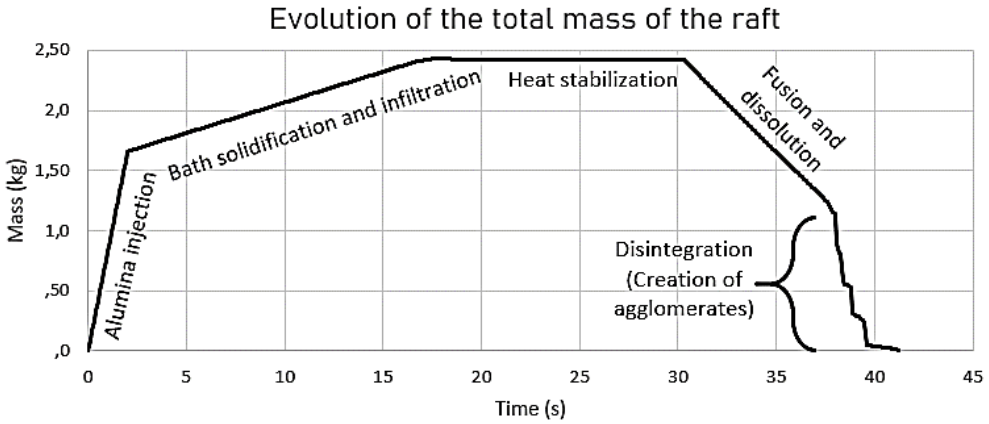

Figure 6. Evolution of the mass of the raft for a specific set of conditions.

This model enables us to create the agglomerates and to know precisely when they should sink to the BMI. It also allows us to determine the moment of the raft disappearance and the variation in aggregate size as they dissolve.

3. Results

The simulations presented in this section illustrate the movement of rafts under different sets of conditions: 1) the time before raft fragmentation (consequence of different injection conditions), 2) the mass injected for each feeding, and 3) the influence of conditions at the bath-metal interface. At this stage of the work, the analysis was performed by looking at all factors individually with the purpose of identifying the dominant behaviors in the movement of solid agglomerates. Further studies will investigate more comprehensively the quantitative effect of each factor and their potential consequence on alumina concentration in the cell, and thus, the potential impact on cell performances.
To perform the analysis, three types of outputs are generated as an outcome of the simulations: the streamlines of the displacement of each individual raft or agglomerate; an image showing the position of each agglomerate at the end of the simulation, and the overall video in a view from above depicting the raft and agglomerate movements. Only the streamlines will be discussed in this article.

3.1 Effect of the disintegration time.

The initial results aim to understand the influence of the time before the disintegration processes begin. As a reminder, the disintegration pattern is influenced by the bath chemistry, the superheat, and the temperature of injection of the alumina. This parameter was investigated due to the strong restriction caused by the anodes in the central channel of the cell at the upper layer of the model. Consequently, the rafts only have the possibility of moving towards the extremities of the cell. The resulting expectation is that when the time is short before the initial disintegration, the raft will distribute agglomerates more evenly along the central channel and enhance the distribution of alumina. In opposition, a longer time before the initial disintegration occurs will lead to additional travel of the raft and will distribute the agglomerates closer to each other, which will lead to a more concentrated distribution of the alumina. The results obtained for fragmentation times of twenty, forty and sixty seconds are presented in Figure 7.

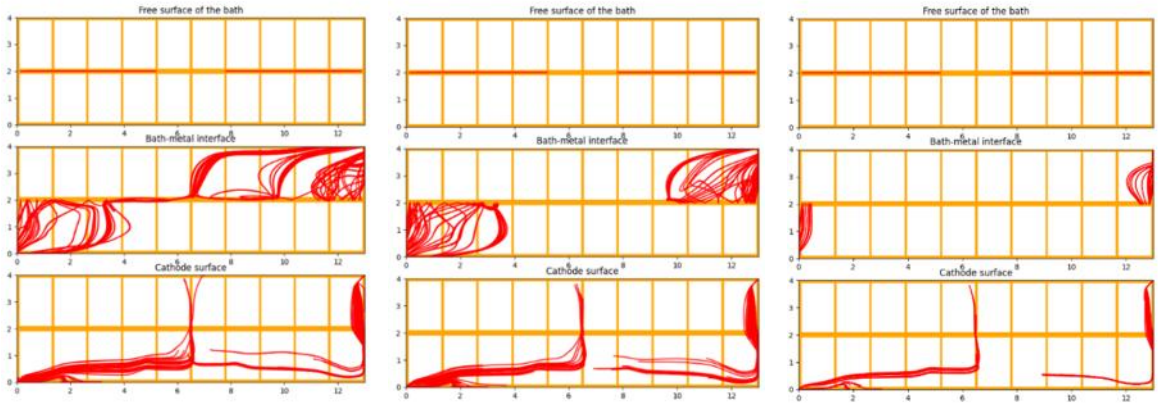

Figure 7: Streamline of the raft movement during 5 minutes for a fragmentation of the raft after 20 s (a), 40 s (b) and 60 s (c).

Following our expectations, as illustrated in the bath-metal interface layer of the three figures, when the time before the fragmentation is reduced (20 s), the agglomerates appear at the BMI earlier and cover a surface of the cell roughly equivalent to 40 % of its surface. On a disintegration time at 40 s, the surface covered by the agglomerates is reduced to 30 % compared to the smaller disintegration time. With a disintegration time at 60 s, the raft moved to the cell boundary with the current bath flow, leading to a negligible coverage of the surface. For conditions with a disintegration time even longer, the result will be similar to the 60 s case as the raft is caught mechanically between the anode and the flow of the current. The interactions between the raft and the crust present in the central channel are not considered in the model which most probably slows down the raft movement towards the extremities.

A longer presence at the BMI has a bigger influence on their movements but also influences their dissolution capabilities. When the agglomerates reach the periphery of the cell, the model considers that they are transported to the lower layer of the model due to the very strong curvature of the metal deformation in these areas. Once in the aluminium, the dissolution process changes drastically and becomes a lot more important than the total time simulated. Consequently, at the end of the simulation, the total mass of agglomerate that remains at the cathode surface represent 13.3 % of the mass injected for a fragmentation occurring after 20 s, 17.3% for a fragmentation after 40 s and 22.3 % for a fragmentation after 60 s. A difference of 4 % between the two first scenarios is quite significant, if it proportionally transposes to 6 tons of alumina which is injected daily in an electrolysis cell. The total sludge formation is consistent, and increasing linearly, with the rafts dissolution time. Additionally, longer dissolution time leads to fewer regions of the cells affected by the dissolution of the aggregates. Therefore, to assure that dissolved alumina is uniformly accessible to the entire cell to sustain electrolysis, a refined study on the transport of dissolved alumina through convection needs to be performed to assess if these conditions may increase the risks of anode effect.

3.2 Effect of the Mass of Alumina Injected

The following results were designed to assess the role of the mass of the raft and its inherent effect on the mass and number of resulting agglomerates. The mass influences the effect of the buoyancy force with the waves and the inertia. It also influences the dynamic of the solidification, fusion, dissolution, and disintegration within the raft. The simulations were carried out with an injection of 0.5 kg, 1 kg and 2 kg in order to evaluate extrema of reasonable operations and to validate if the behavior is non-linear. The alumina feeding remains constant in each case close to the

theoretical value of 1 kg/min per feeder. The time and number of agglomerates formed is an output of the heuristic model and will lead to different numbers of agglomerates, with different masses, generated for each simulation.

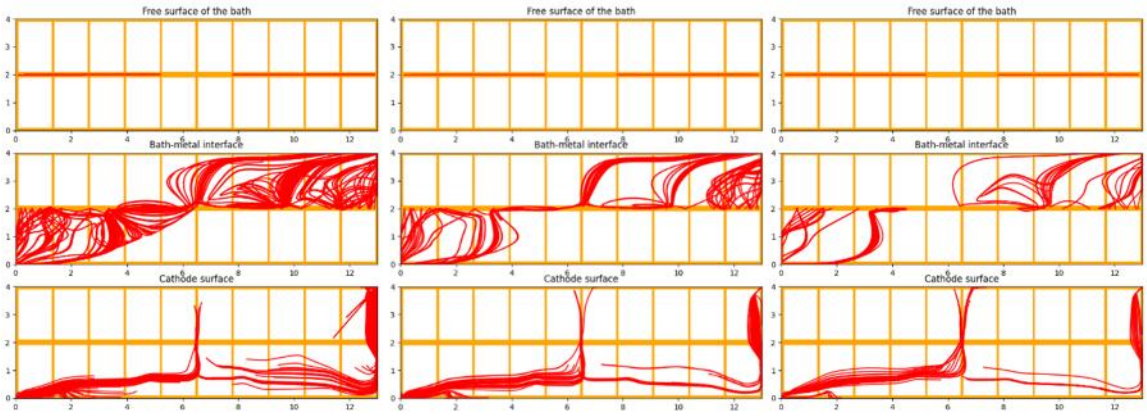

Figure 8: Streamline of the raft movement during 5 minutes for an injection of 0.5 kg (left), 1 kg (middle) and 2 kg (right) of alumina.

The results show that increasing the injected mass of alumina leads to agglomerates with an individual mass that becomes larger on average. Consequently, the displacement of the agglomerates will be less influenced by the MHD current due to their size, resulting in a less significant dispersion at the bath-metal interface. Inherently, due to an increased mass to dissolve, they will however tend to be present for longer at the BMI with a greater chance of reaching the periphery of the cell. Conversely, smaller agglomerates travel quicker but also dissolves more quickly.

Following the 5 minutes of simulation, the proportion of the injected mass present on the cathode surface is 9.3 % for injections of 0.5 kg, compared with 13.3 % for injections of 1kg and 17.2 % for injections of 2 kg. It is also possible to see that the overall surface affected by the dissolution of agglomerates is more important for smaller injections. Therefore, injecting smaller doses appears to be beneficial for the electrolysis process and it can limit the total mass of alumina migrating to the cathode, despite the increased frequency of feedings that are necessary. Finally, the results also show that the effect observed is non-linear and by comparing the difference between 0.5 kg, 1 kg and 2 kg, it is possible to observe that the median case (1 kg), which is a standard of the industry, appears to already be above the optimal threshold. Further study will be necessary to try and pinpoint the recommended weight of injection, while taking into consideration the other operational and maintenance costs associated to an increased feeding frequency.

3.3 Effect of the Conditions at the Bath-Metal Interface

The following results was designed to assess the role of the individual elements that shape of the bath-metal interface on the movement of agglomerates. As observed in the previous sections, rafts appear attracted towards the corners of the cells due to the permanent deformation. The following results show the movement of rafts for 3 minutes for two idealistic cases. The first one being without the presence of waves at the BMI and the alternate scenario being without the presence of a permanent deformation. In both cases, the MHD flow at the BMI was active.

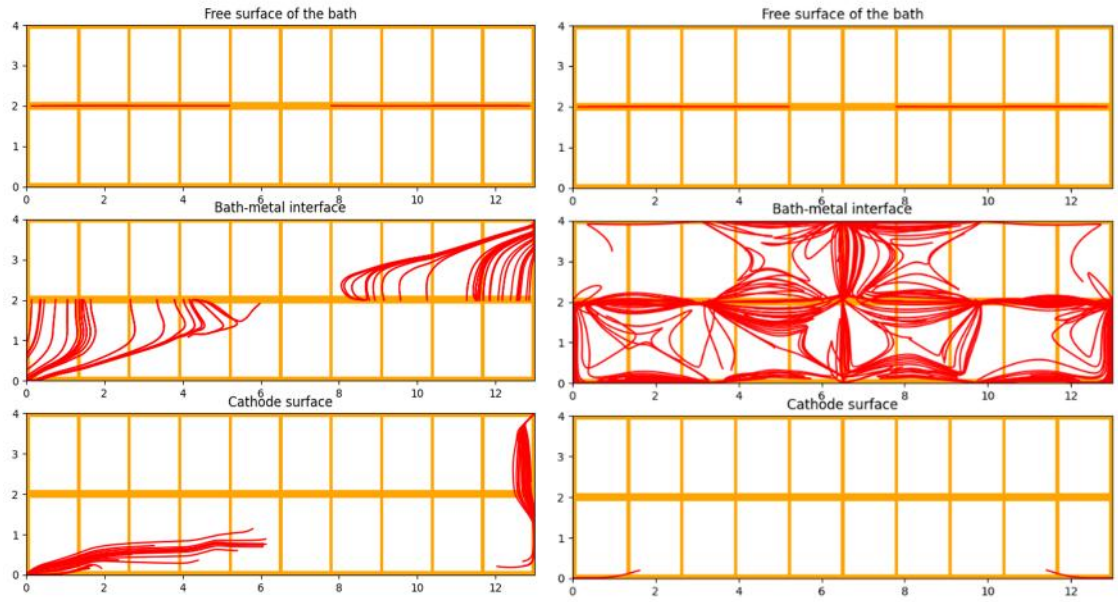

Figure 9: Streamline of the raft movement during 3 minutes for only the permanent deformation at the BMI (left) and only the formation of wave at the BMI (right).

The results clearly illustrate that the permanent deformation of the cell is the main driver in the movement of rafts at the BMI. While figure 8 (left) illustrates that roughly only 40 % of the surface of the BMI is in contact with the agglomerates, this value rises to 75 % of the surface of cell being in contact with agglomerates in the second scenario. While the second case results can be influenced by the timing of the injections and the wave initial position, the difference between both cases is striking.

Ultimately, this different behavior can significantly impact the formation of sludge as all the rafts are pushed towards the corners, enabling them to migrate to the surface of the cathode. If only the presence of waves is considered, it prohibits the formation of sludge as the aggregates will move freely at the bath-metal interface without being trapped at the periphery of the cell. Nonetheless, further improvements to the model will consider that potential combination of additional factors such as the buoyancy, the surface tension, the kinetic energy and the size of agglomerates may lead to the penetration of the BMI leading to additional sludge formation. Following these model modifications, the overall sludge formation is expected to increase in both scenarios but the permanent deformation will remain the main contributor to the sludge formation.

3.4 Discussion on the Risk of Sludge Formation

The presented outcome obtained from all three result sections highlight the importance of understanding the mechanics of raft movements, especially in the periphery of the cell as it may be a dominant factor influencing the sludge formation. As presented, this study considers only the horizontal movements of these rafts (excluding the vertical migration between different layers), but the reality is three-dimensional and the rafts are free to move vertically if the balance of forces justify such movements. While the behavior at the cell periphery is logical due to the interface curvature, further investigation is necessary to prove the hypothesis that this automatically generates sludge. It is important to consider the conflicting film flow moving upward from the cathode to the electrolytic bath that has been presented by some authors [18-20]. Therefore, the

exact final position of these agglomerates is most probably dependent on a wide variety of factors such as the return flow velocity, the size of the agglomerates, the deformation curvature, their kinetic energy, and others. Although, the most likely scenarios are that these agglomerates remain either caught in the cell curvature until they are completely dissolved, or they pierce the BMI and move to the cathode surface. In both cases, the contribution of these agglomerates to the global alumina distribution in the cell will be strong and negative. Therefore, efforts to mitigate these occurrences should be preserved.

4. Conclusions

A new approach has been developed to simulate the transport of rafts and aggregates by simplifying the aluminum electrolysis cells into three parallel planes representing the free surface of the bath, the bath-metal interface, and the cathode surface.

This model simulates the interaction of the raft and the flow at the bath surface via drag force. The flow at the bath-metal interface is based on a simulation of magnetohydrodynamic forces coupled with permanent deformation and waves. This flow acts on the raft with drag force and buoyancy force. The flow at the cathode surface is identical to the flow related to the magnetohydrodynamic forces present at the bath-metal interface.

The model also uses the results from a heuristic model that determines the evolution of a raft's mass after alumina injection. It also determines the specific timeline for the disintegration of the raft into aggregates that will sink to the bath-metal interface.

The obtained results show that the time between raft formation and the start of disintegration impacts the drop-off point of aggregates at the bath-metal interface. They will move differently, and the formation of sludge on the cathode can be influenced.

The results obtained from the study on the impact of the injected mass on the movement of rafts show that as the injected mass increases, the individual masses of the aggregates become larger. Consequently, waves have a greater influence on their movement, and their dissolution is less pronounced. The results indicate an increase in the mass of produced sludge and also illustrates that the commonly injected mass of 1000 g is above an optimal threshold.

Permanent deformation is the studied factor that promotes raft movement towards the corners of the cells, which in turn is very likely a strong contribution to sludge formation.

This model is still under development, but it already highlights key behaviors that can pinpoint potential solutions with significant gains in the process. Additional tools such as this one are critical to achieve the proper understanding related to alumina distribution, which is required for optimal operation in the present era of low energy consumption. Such knowledge is key to maintain optimal operational standards and also to maintain anode effects frequency and sludge formation at minimal possible levels.

5. References

1. Heuristic alumina dissolution model, Université du Québec à Chicoutimi, Polytechnique de Montréal, and Rio Tinto, 2016-2023.
2. Valdis Bojarevics, In-line cell position and anode change effects on the alumina dissolution, *Light Metals* 2021, 584-590.
3. Xiaozhen Liu et al., CFD modeling of alumina diffusion and distribution in aluminum smelting cells, *JOM*, 2019. 71(2): 764-771.

4. Vladis Bojarevics and Marc Dupuis, Advanced alumina dissolution modelling, *Ligth Metals*, 2022, 339-348.
5. Thomas Richer et al., Improvements to a mathematical model used to reproduce the wave and stream at the bath-metal interface and assess their impact on the movement of alumina rafts, *Ligth Metals*, 2023, 757-764.
6. Thomas Richer et al., Mass Transport by waves: physical model with coalescence, fragmentation, and displacement on a bath-metal interface, *Ligth Metals*, 2022, 371-380.
7. L. Rakotondramanana et al., Mass Transport by waves on the bath metal interface in electrolysis cell, *Ligth Metals*, 2020, 510-516.
8. L. Rakotondramanana et al., Mass Transport by waves: bath-metal interface deformation, rafts collision and physical model, *Ligth Metals,* 2021, 344-350.
9. Jonathan Alarie et al., Influence of additives on alumina dissolution in superheated cryolite melts, *Ligth Metals,* 2021, 533-540.
10. Véronique Dassylva-Raymond, *Analyse et modélisation du comportement des agrégats d'alumine dans le procédé Hall-Héroult*, Thèse de doctorat, Université du Québec à Chicoutimi, 2015.
11. Thomas Roger et al., Modeling of the heat exchange, the phase change, and dissolution of alumina injected in electrolysis cells, *Ligth Metals,* 2022, 363-370.
12. COMSOL Multiphysics® v. 6.1.
13. Andrey Zavadyak et al., Transfer processes in the bath of high amperage aluminium reduction cell, *Ligth Metals*, 2019, 773-777.
14. Hongliang Zhang et al., Numerical simulation of alumina-mixing process with a multicomponent flow model coupled with electromagnetic forces in aluminum reduction cells, *JOM*, 2014, 66(7): 1210-1217.
15. Ted Belytschko, Wing K. Liu and Mark O'Neal, Contact - impact algorithms for penetration studies. *U.S. Army Research Office*, 1990.
16. Csilla Kaszas, *Behaviour of alumina powder fed into molten electrolytic bath*, Thèse de doctorat, Université du Québec à Chicoutimi, 2020.
17. Jonathan Alarie et al., Validation of the gravimetric method to properly follow alumina dissolution in cryolitic bath, *Ligth Metals* 2020, 680-687.
18. Mojtaba Fallah Fini et al., Sludge formation in hall–héroult cells: drawbacks and significant parameters, *Mineral Processing and Extractive Metallurgy Review*, 2020. 41(1): 59-74.
19. Asbjørn Solheim, Nils-Håvard Giskeødegård and Nancy J. Holt, Sideledge facing metal in aluminium electrolysis cells: freezing and melting in the presence of a bath film, *Light Metals* 2016, 333-338.
20. Torstein Hansen, Asbjørn Solheim and Kemal Nisancioglu, Hydrodynamic model for the bath film between metal and side ledge in aluminum cells, *Light Metals* 1996, 351-356.